Similarity measures for identifying material parameters from hysteresis loops using inverse analysis

**Charles F. Jekel · Gerhard Venter ·
Martin P. Venter · Nielen Stander ·
Raphael T. Haftka**

Abstract Sum-of-square based error formulations may be difficult to implement on an inverse analysis consisting of multiple tension-compression hysteresis loops. Five alternative measures of similarity between curves are investigated as useful tools to help identify parameters from hysteresis loops with inverse analyses. A new algorithm is presented to calculate the area between curves. Four additional methods are presented from literature, which include the Partial Curve Mapping value, discrete Fréchet distance, Dynamic Time Warping, and Curve Length approach. These similarity measures are compared by solving a non-linear regression problem resembling a single load-unload cycle. The measures are then used to solve more complicated inverse analysis, where material parameters are identified for a kinematic hardening transversely anisotropic material model. The inverse analysis finds material parameters such that a non-linear FE model reproduces the behavior from five experimental hysteresis loops. Each method was shown to find useful parameters for these problems, and should be considered a viable al-

C. F. Jekel *corresponding author*
Department of Mechanical and Aerospace Engineering, University of Florida, Gainesville, FL 32611, USA
E-mail: cj@jekel.me E-mail: cjekel@ufl.edu

G. Venter
E-mail: gventer@sun.ac.za
Department of Mechanical and Mechatronic Engineering, Stellenbosch University, Private Bag X1, Matieland, 7602, South Africa

M. P. Venter
E-mail: mpventer@sun.ac.za
Department of Mechanical and Mechatronic Engineering, Stellenbosch University, Private Bag X1, Matieland, 7602, South Africa

N. Stander
E-mail: nielen@lstc.com
Livermore Software Technology Corporation, Livermore, CA 94551 USA

R. T. Haftka
E-mail: haftka@ufl.edu
Department of Mechanical and Aerospace Engineering, University of Florida, Gainesville, FL 32611, USA

ternative when sum-of-square based methods may be difficult to implement. It is important to consider multiple similarity measures in cases when it is impossible to obtain a perfect match.

1 Introduction

The calibration of model parameters to find models which reproduce experimental hysteresis tension-compression cycles is difficult. There are a wide variety of material models implemented in commercial finite element (FE) software. Unfortunately the selection of appropriate parameters for these models is not a simple process, despite the advancements in experiential methods, constitutive models, and the FE method. In some applications constitutive parameters can be determined by a curve fit from experimental data as done with a number of generalized polynomial strain energy models [1]. Alternatively full-field displacement methods provided by non-invasive optical techniques have been used with the virtual fields methods to identify constitutive parameters [2, 3]. Another solution has been to use an inverse analysis to identify material parameters in a process of updating a FE model, where material parameters are determined such that the FE model's response best replicates an experiment. The focus of this paper is on the objective function that quantifies the quality of fit between two different responses.

In this context an inverse analysis refers to the process of using optimization to minimize the difference between experimental data and a numerical model's response. Some objective function is used to quantify the differences between responses. A few of the first works related to inverse analysis to determine material parameters include [4, 5, 6, 7, 8]. For various hysteresis and hardening parameter identification problems, objective functions based on the sum-of-squares have been used. While the use of a sum-of-squares objective function is widely established, other similarity measures may be easier to work with when dealing with experimental hysteresis loops.

It is well-established to use a sum-of-square based objective function with inverse analysis to identify material parameters. Lederer et al. [9] used a root means square quality function to measure the difference between experimental and numerical magnetic hysteresis curves. Haddadi et al. [10] used a form of mean square error as the cost function to identify kinematic hardening and micro-structural model parameters. The mean square error compared the difference of stress and hardening rates between a FE model and experimental data. Eggertsen and Mattiasson [11] used a weighted mean square error to identify material parameters for hardening laws with an inverse analysis. Harth et al. [12] described using a weighted sum of differences between experimental and numerical models to identify the optimum material parameters for inelastic constitutive models. Rabahallah et al. [13], Souto et al. [14], Yoshida et al. [15] used a weighted sum-of-squares objective function to identify material parameters from inverse analysis on hysteresis loops. De-Carvalho et al. [16] concluded that a weighted sum-of-squares objective function was more appropriate than a single point objective function for complicated geometric phenomena including necking, springback, and stress concentration.

A typical sum-of-squares is defined as

$$SS = \sum_{i=1}^{n} \left(f(x_i) - \hat{f}(x_i) \right)^2 \qquad (1)$$

where f is the experimental data, $\hat{f}$ is the numerical model, and the difference is taken at the same x_i condition. Often differences in stress between the experimental and numerical data are calculated for the same strain values [10, 14, 16, 17, 18].

Now consider the simple example in Fig. 1 of some potential noisy material load-unload response accompanied with a numerical model that replicates that response. Initially in (a) it may appear trivial to apply the sum-of-squares, though when zooming into the data as shown in (b) it appears that the experimental data does not share mutual strain or stress values in order to calculate the sum-of-squares. There is essentially no concurrent x_i to calculate the difference between the experimental data and numerical model.

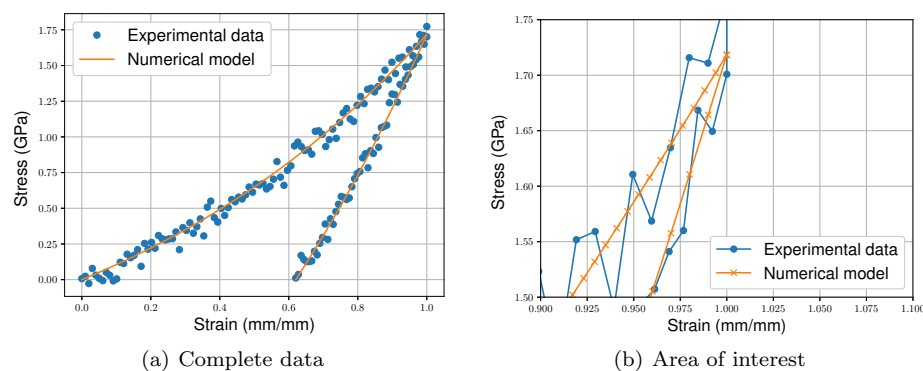(a) Complete data   (b) Area of interest

Fig. 1 Example of a potential material load-unload response and the numerical model replication of the response where (a) shows the complete data while (b) shows a zoomed-in area of interest and the order of the experimental data points.

A tension-compression-tension test with experimental data and the results from a numerical model is shown in Fig. 2. There exists some set of numerical model parameters which will result in the numerical curve aligning with the experimental curve exactly. Often, an optimization is run to find the best set of parameters that minimize the error between two curves. Traditionally the error has been defined as a sum-of-square based objective function. However, in this case it is not possible to directly apply a sum-of-squares function to quantify the difference between the numerical model and experimental data. One problem is that there are a different number of data points on the experimental curve than the numerical curve. Additionally, there are no concurrent stress or strain values to take a difference of as required by a sum-of-squares function. An alternative objective function is needed to measure the similarity between the two curves.

Several other methods have been proposed in response to the shortcomings of using sum-of-squares to identify parameters from hysteresis loops. These methods will be discussed in detail in Section 2. A new algorithm to calculate the area
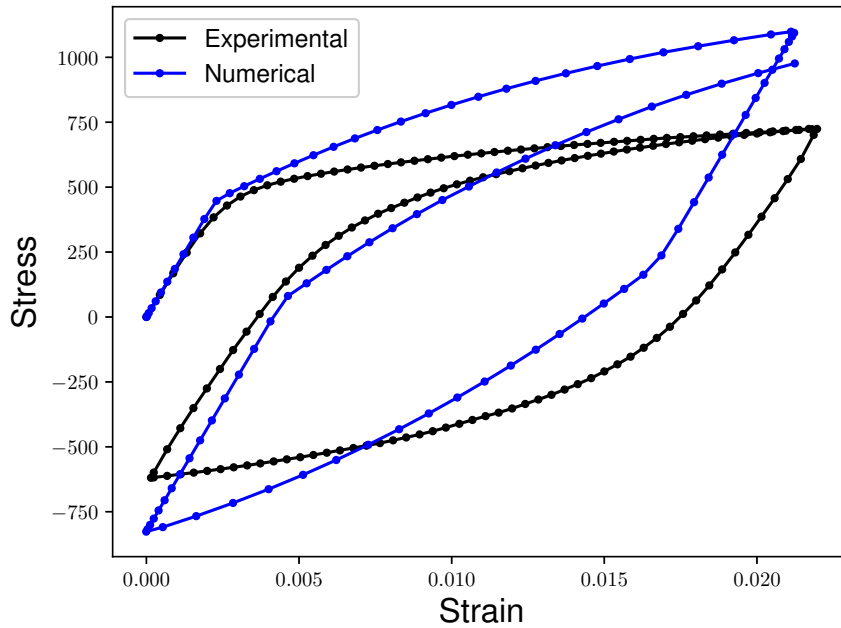
Fig. 2 Assessing the quality of the numerical model's match of the experimental response is difficult for material tension-compression-tension curves.

between curves is proposed and compared with other measures of similarity from literature. The area algorithm is compared to the discrete Fréchet distance, Dynamic Time Warping (DTW), Partial Curve Mapping (PCM), and a Curve Length based objective function. The measures of similarity are minimized on simple problems where it is impossible for the model to match the data exactly. Additionally, these measures are used as the objective function in an inverse analysis to determine material parameters for a kinematic hardening transversely anisotropic material model. The resulting FE models replicate the experimental data from five hysteresis tension-compression loops. Artificial noise is added to the problems to demonstrate the robustness of the measures to noise, and to help distinguish the measures in an events where it is impossible to match experimental data exactly.

2 Methodology

Inverse analysis have been used to identify material parameters for numerical models [10, 11, 12, 13, 14, 15, 19, 20]. In general some experiment was conducted on a material (e.g. a load-unload uniaxial test, or tension-compression test). Then a numerical model was created which replicates the physical conditions of the test (e.g. an appropriately constrained FE model). In the case of using a FE model, this process has been referred to as the FE model updating (FEMU) method [21]. An inverse analysis determines parameters of the numerical model by minimizing the difference between experimental data and the response of the numerical model. Optimization is used to find the parameters by minimizing an objective function

which describes the quality-of-fit from the collection of parameters. Traditionally the objective function has been based on a sum-of-squares error formulation when using an inverse analysis to find material parameters. This work explores using Partial Curve Mapping (PCM), Area between curves, discrete Fréchet distance, Dynamic Time Warping (DTW), and a Curve Length objective function proposed by Andrade-Campos et al. [22] as measures of the similarity between two curves for inverse analyses.

It is important to distinguish between the inverse analyses that require a FE model to continuously update, and non-linear regression problems which parameters are identified from curve fits to experimental data. There are a number of generalized polynomial strain energy models (including MooneyRivlin and Ogden hyperelastic material models) which can be identified from curve fits [1]. Additionally, Martins et al. [23] used non-linear regression to determine properties of various hyperelastic models for soft tissues.

There have been a variety of optimization techniques used to solve inverse analysis and non-linear regression problems, including both stochastic and deterministic optimization methods [24]. The focus of this work is to present a collection of objective functions that may be particularly useful when performing an inverse analysis to identify material parameters from hysteresis loops. Thus any optimization technique could be used, assuming the result is close to the global optimum. It is worth to note that different optimization techniques which appear to solve some inverse analyses well, may struggle on other particular inverse problems as principle of the No Free Lunch theorem [25]. LS-OPT® [26], a general purpose design optimization and probabilistic analysis toolbox, was used to solve the inverse analyses for this study.

Three problems are proposed and solved in this paper by minimizing the PCM, Area, discrete Fréchet, DTW, and Curve Length measures. The first problem illustrates the differences between these similarity measures and a traditional least squares fit when fitting a line to quadratic data and fitting a line to data with an outlier. The second problem is a non-linear regression problem invented to illustrate finding material parameters from a single load-unload cycle. The third problem is an inverse analysis to identify material parameters for a kinematic hardening model. Separate optimizations are performed using either the PCM, Area, discrete Fréchet, DTW, or Curve Length similarity measures as the objective function. The intention is to demonstrate how each measure may be useful when identifying material parameters. The methodology goes on to describe the PCM, Area, Fréchet, and DTW measures of similarity between two curves. It is important to note that the order of the data points is important for these methods[1].

2.1 Partial Curve Mapping

The Partial Curve Mapping (PCM) method was proposed by Witowski and Stander [27] to identify material parameters with inverse analyses. PCM uses a combination of arc-length and area to determine the similarity between curves, because

---

[1] Initially consider two identical curves discretized by identical data points. All of these measures of similarity would return a value of zero. Now reverse the order of the data points on one curve, and then all of these measures would return a large value.

sometimes the choice of parameters changes the overall curve length. An example of where an experimental curve and numerical curve have different overall lengths is seen in the material tension-compression-tension test of Fig. 2. First the arc-length of the shorter curve is imposed onto a section on the longer curve. Then trapezoids are constructed between the curves, and the areas of the trapezoids are summed. This is repeated for 200 or so iterations, as various offsets of the short arc length are imposed on the curve with the longer arc length.[2] Trapezoids constructed between two curves for an arbitrary offset can be seen in Fig. 3. The final PCM value is the minimum area from all attempted arc-length offsets.
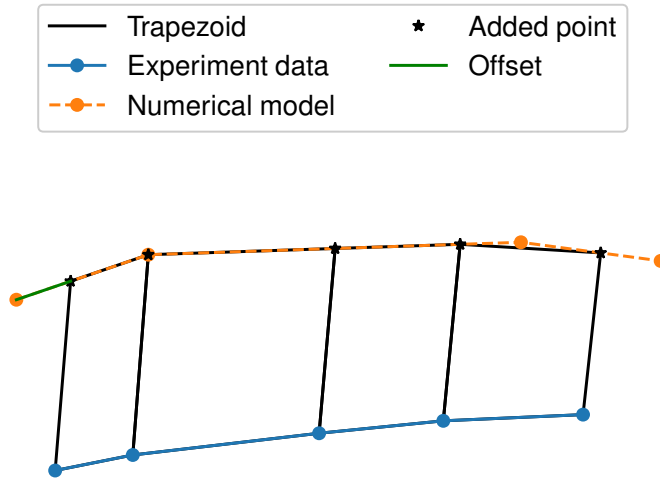

Fig. 3 The PCM method constructs trapezoids between the two curves for every possible offset.

The PCM algorithm is implemented in LS-OPT and has been used to calibrate a variety of material parameters. Venter and Venter [28] used the PCM method with an inverse analysis to calibrate a hybrid material model capable of reproducing the orthogonal load-unload response for plain woven polypropylene. ul Hassan et al. [20] used the PCM method to calibrate material parameters for the same kinematic hardening model (MAT_125) used in Section 3.3. In LS-OPT PCM is referred to as a curve matching algorithm [26].

Though the PCM method has proven a useful tool for material calibration problems, there are some limitations. The PCM method performs poorly when the data has noise, as noise artificially increases the arc length. The LS-OPT

---

[2] Arc lengths can be iterated such that for the first iteration the arc length of the longer curve is only considered from the beginning of the data to the end of the arc length on the shorter curve. The next iteration would again consider only the shorter arc length of the longer curve, but only after some offset from the beginning of the longer curve. The process is repeated until an offset is used such that the last data point of each curve is considered.

manual recommends to reduce noisy data with a filter prior to using the PCM method [26].

2.2 Area between two curves

Two curves are generally discretized into a time-series of ordered data points. An algorithm is proposed in this paper to approximate the area between two curves. The algorithm constructs quadrilaterals between two curves and calculates the area for each quadrilateral. The details of the area algorithm is presented in Appendix A.

Two curves that are being compared require the same number of points in order to construct quadrilaterals to approximate the total area between curves. If one curve has fewer data points than the other curve, data points are added until both curves have the same number of data points. It was chosen to add, rather than remove points to avoid any loss of information for general problems. While there are many ways to add artificial data points to the curve, a simple approach was taken which adds an artificial data point by bisecting two points. The location for the bisection was chosen based on the largest Euclidean distance between two consecutive points. Points are added to the curve in this fashion until both curves have the same number of points.

Polygons assume that there is a straight line between any two points. This straight line assumption is important, because adding additional points through the linear interpolation doesn't change the area between the two curves. For instance you can split a pentagon into two quadrilaterals, and the area of the two quadrilaterals will be exactly equal to the area of the pentagon. The adding of additional points is just used to aid in the facilitation of the area approximation. As the number of data points on both curves increases, so does the accuracy of the area approximation.

A simple demonstration of the Area method is shown in Fig. 4, where quadrilaterals are constructed between experimental and numerical data. The numerical simulation yields four data points while the experimental data has five points. An artificial data point was added to the numerical data by bisecting the two consecutive points with the largest Euclidean distance, such that both curves have the same number of points. Four quadrilaterals are then created between the curves by taking consecutive pairs from each curve. Since each quadrilateral is a simple quadrilateral, Gauss's area formula is used to calculate the area of each quadrilateral. The quadrilateral areas are summed to give the effective area between curves.

The area between two curves is a positive value ($A \geq 0$). This is true even when the two curves considered cross each other. It is possible for a curve that is slightly above the desired curve to have the same value as a curve that is slightly below the desired curve. Whether the curve is over or under the desired curve doesn't matter, however what does matter is the amount of mismatch between the two curves. Minimizing the area between the two curve results in minimizing the amount of mismatch between two curves.
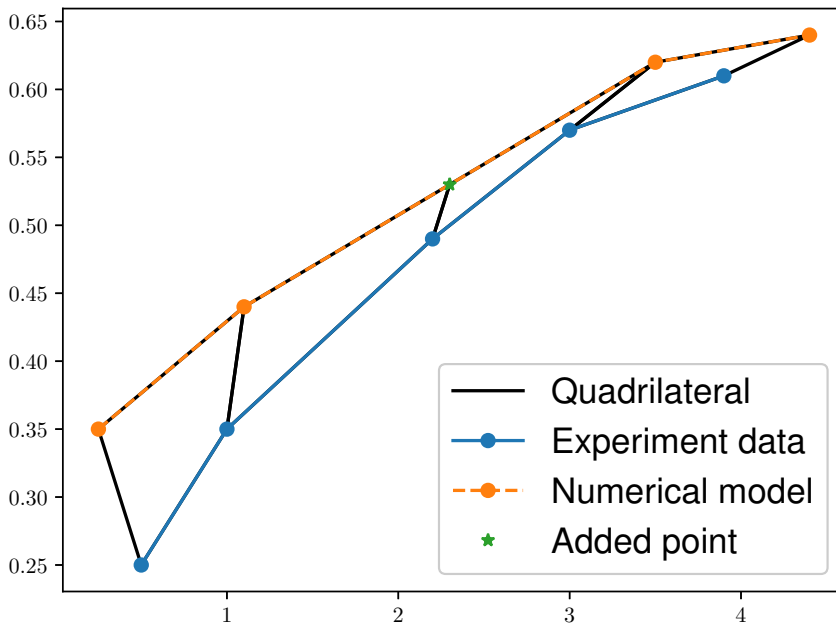
Fig. 4 The Area between two curves is approximated by summing the quadrilaterals. An artificial point is added to the numerical model, such that both curves have the same number of points.

2.3 Fréchet distance

The Fréchet distance is a measure of similarity between curves which preserves the time-series order of data along the curves. The measure was first defined in Fréchet's PhD thesis [29]. Intuitively the Fréchet distance has been described as the length of a leash in a walking dog problem. Suppose a man is walking a dog, where the man is constrained to stay on one curve and the dog on another. The man and dog can vary their velocities independently at all times. Both the man and the dog are limited to either moving forward or stopping along their curves, as it is forbidden for them to move backwards. The Fréchet distance reflects the shortest possible leash connecting the man and dog sufficient to complete the walk along the curves.

Eiter and Mannila [30] described an algorithm to approximate the Fréchet distance by considering the line segments between the end points of two polygonal curves. This algorithm is referred to as the discrete Fréchet distance, or the coupling distance. If we are to consider a curve P with p number of points and a curve Q with q number of points, the discrete Fréchet distance has a fixed quadratic run time of $O(pq)$. There has been work to reduce the quadratic run time cost of the discrete Fréchet distance [31, 32]. The computational cost is generally not a concern when considering a typical test data, and is only mentioned to understand how the algorithm scales with the number of data points. The discrete Fréchet

distance has been used in a variety of applications, including the identification of unique atomistic motions [33].

The difference between the discrete Fréchet distance and the true Fréchet distance is at most the length of the longest edge along the polygonal curves [30]. It is worthwhile to note that algorithms to obtain a more accurate Fréchet distance do exist, but at the cost of additional computational expense. For instance Alt and Godau [34] presented an algorithm that computes the Fréchet distance using a parametric search with a run time of $O(pq \log(pq))$. The discrete Fréchet distance was deemed to be a reasonable approximation for this work because the upper bounded error was small with the provided data. The Python MDAnalysis library includes a discrete Fréchet distance function that was used in this work [33].

2.4 Dynamic Time Warping

Dynamic Time Warping (DTW) has been a popular method for pattern recognition, and particularly useful for speech recognition [35, 36]. DTW first calculates the distance between points of one curve onto the other curve. If we are to consider a curve P with p number of points and a curve Q with q number of points, for each p point the distance between p and every q point is calculated. This has the same quadratic complexity of $O(pq)$ as the discrete Fréchet distance. The goal of DTW is to find the path between curves that minimizes the cumulative distance between points.

Imagine traversing the path of both curves simultaneously, where you start from the first index of each curve. The distance between the points at the first index of each curve is your first distance. You are then presented with three choices: (1) move to the second index of curve P, (2) move to the second index of curve Q, or (3) move to the second index of curve P and the second index of curve Q. The second distance will be either the distance between the points of the second indexes, or the distance between the point of the second index on one curve and the first index on the other curve. This process is repeated until you are on the last index of each curve. The optimal DTW distance represents the path with the smallest cumulative distance once you have reached the last index of each curve. To aid in the visualization of DTW consider the arbitrary curves in Fig. 5 a. The optimal DTW path is shown in Fig. 5 b, where the DTW distance is the value of the tile in the top right (at the last index of each curve).

The R *dtw* package was used in this work [37]. In a case where a very large number of points are considered, it may be worthwhile to consider the FastDTW algorithm by Salvador and Chan [38]. FastDTW is a popular approximation of the DTW distance with linear cost, although the reduced computational expense comes at the cost of reduced accuracy. The quadratic computational expense is not a concern for typical hysteresis curves, but it is worthwhile to note how the method may scale provided a very large number of points.

2.5 Curve Length

Cao and Lin [39] suggested an objective function with automatic weighting factors to determine material constants that match experimental data. Andrade-Campos
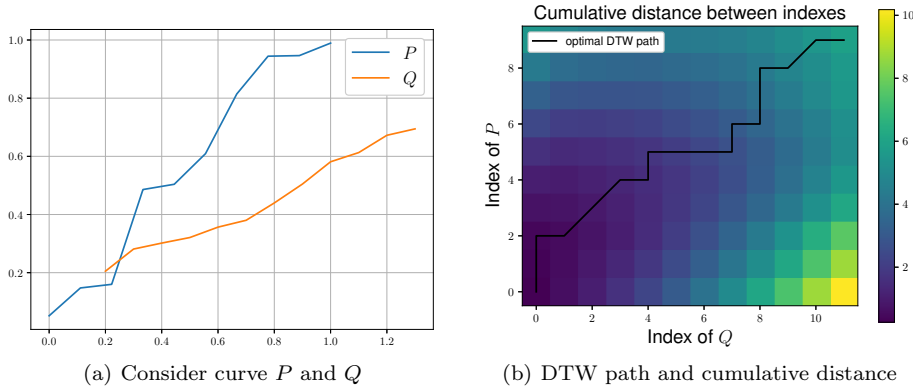
(a) Consider curve P and Q

(b) DTW path and cumulative distance

Fig. 5 Arbitrary curve P and curve Q shown in two dimensions in (a) where the optimal DTW path is shown in (b) where each tile represents the cumulative distance from the first index of each curve.

et al. [22] took the objective function of Cao and Lin and extended it to be applicable for negative and zero stress and strain values. Additionally, Andrade-Campos et al. introduced a novel curve length attribute to be included in the objective function to quantify the quality of fit between two curves. The final Curve Length objective function is suitable for identifying parameters for a variety of cases, including cyclic hysteresis tests and Bauschinger tests.

This Curve Length inspired objective function works on the principle that a point on one curve can be compared to its corresponding curve length location on the other curve. Essentially the stress and strain values from a cyclic tension-compression-tension test can be expressed as a function of the curve length distance from the first data point. A data point on the experimental curve will have some curve length distance that can be expressed as a ratio from the total experimental curve length. The stress and strain values from two curves are compared at the same curve length ratios, and an objective function is formulated as the sum of the natural log of these squared deviations.

An illustration depicting this process is provided in Fig. 6. A corresponding data point on the numerical model is calculated at the equivalent curve length location of the experimental curve. Squared residual values are then calculated as function of both the dependent and independent variables. The sum of these squared residuals is used to quantify the difference between the two curves.

The implementation of the Curve Length measure used in this work is the OF2 from [22], which was seen to better identify a hyperelastic and elasto-viscoplastic models. This formulation is self-normalizing, and utilizes a natural log transformation. This OF2 objective function is referred to as the Curve Length method throughout this paper.

3 Results

The different similarity measures were first compared to minimizing the sum-of-squares to clearly illustrate the difference between methods. The first example
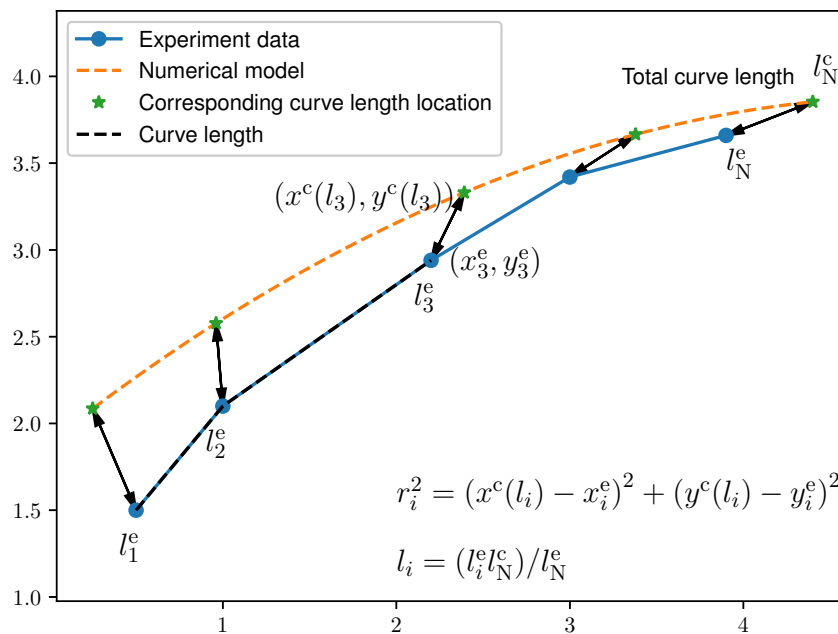
Fig. 6 Depiction of a Curve Length inspired objective function. The r_i^2 residuals are summed for the N data points to quantify the difference between the two curves.

fits a straight line to linear data with a single outlier and fits a straight line to quadratic data. Optimization is used to find the best line according to the Area, PCM, discrete Fréchet, DTW, and Curve Length similarity measures.

The similarity measures were then used in optimizations to identify parameters from a single load-unload cycle. This problem was invented for the purpose of illustrating the methods on a simple example. There is a known analytical solution. Having a known solution makes it easier to test both the optimization strategy, and the implementation of each similarity measure.

Lastly, material parameters were identified for a kinematic hardening transversely anisotropic material model. Optimization was used to find the parameters such that the FE models reproduce experimental tension-compression-tension cycles. Test data is from five different tension-compression-tension cycles. The material exhibits stress-strain hysteresis, and the results compare the differences between measures of similarity. To see how the objective functions deal with noise, the inverse problems are solved again with artificially added noise to the desired curves.

In general, it is impossible for numerical models to match experimental data exactly. It is not likely that a material model matches reality perfectly, and even if it does, measurement errors are likely to foil a perfect fit. An outlier, linear model to quadratic data, fitting with noise, and the kinematic hardening problem are just examples of when obtaining a perfect fit is not possible. These examples illustrate how the best model may be dependent upon the similarity measure chosen for many practical problems.

3.1 Straight line illustrative fit

In this section a straight line is fit to linear data with an outlier, and to quadratic data using the five measures of similarity. The fits are performed using a global optimization routine. The similarity measures were minimized using the genetic algorithm (GA) implemented in LS-OPT with the default parameters. The GA serves as the global optimization routine to find the best line.

A straight line was fit to ten data points originating from a straight line, with one of the data points being modified to resemble an outlier. The Area, PCM, discrete Fréchet, DTW, and Curve Length similarity measures were minimized to find the line of best fit to the data. The methods are compared to the line resulting from minimizing the sum-of-squares through a least squares fit. Results from the different similarity measures are presented in Fig. 7. The Area and DTW methods entirely ignore the single outlier, as expected between methods that sum the absolute distances (L1 norm). Minimizing the discrete Fréchet distance creates a line that is in-between the outlier and the remaining data points, as can be expected by a method that minimizes the maximum distance (L-infinity norm). Minimizing the PCM method produced a line with a steeper slope than the trend, as the method was accounting for the increased arc-length from the outlier. The sum-of-squares optimum represents a line that is an average preserving compromise between the true trend and the outlier, as expected from an L2 norm. The Curve Length similarity measure produces a line that is initially similar to the sum-of-squares optimum, but dips slightly below the data points at the end.

The results of fitting a line to quadratic data are shown in Fig. 8. First a fit was performed to the original data. Then a second fit was performed, where the data was first normalized such that each variable ranged from zero to one. The fits were determined by minimizing the similarity measures with the GA. The discrete Fréchet distance and DTW methods were severely affected by the normalization. Looking at the normalized quadratic data it is seen that the discrete Fréchet distance resulted in a line that was just above the sum-of-squares solution, while the Area and DTW methods result in a line just bellow the sum-of-squares solution. Minimizing the Area and DTW produced the same results when fitting quadratic data or fitting a line with an outlier, as seen in Fig. 7 and Fig. 8 (b). The PCM method resulted in a line with a different slope than the other methods. Normalization is built into the PCM and Curve length methods, so in both cases they resulted in the same fit. Normalization did not appear to affect the Area method as the results with and without normalization were the same.

3.2 Single load-unload cycle example

A single load-unload cycle problem is proposed as the following piecewise equation

$$\begin{cases} \exp(\beta_0 x) + \beta_1 & 0 \leq x \leq 1.0 \\ 2.0\exp(\beta_2 x) - 2.0\exp(\beta_3) + \exp(1.0) - 1.0 & 1.0 \geq x \geq 0.62 \end{cases} \qquad (2)$$

with four unique $\boldsymbol{\beta}$ parameters to identify. This piecewise function with added noise was seen in Fig. 1. The true values and optimization bounds of the problem are found in Tab. 1. The problem is solved with and without noise. Artificially
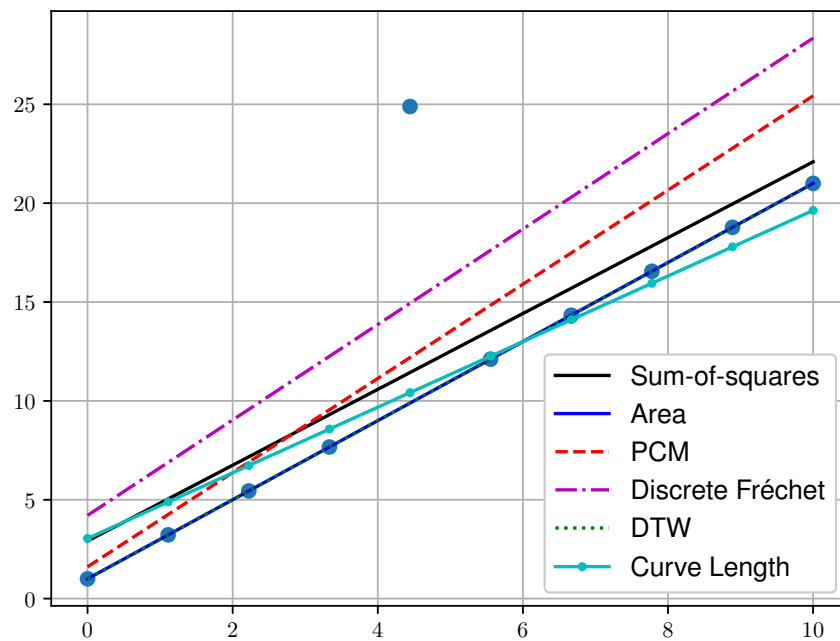
Fig. 7 Results of fitting a line to linear data with central outlier by minimizing different similarity measures. The outlier was exaggerated to clearly show the differences between similarity measures.
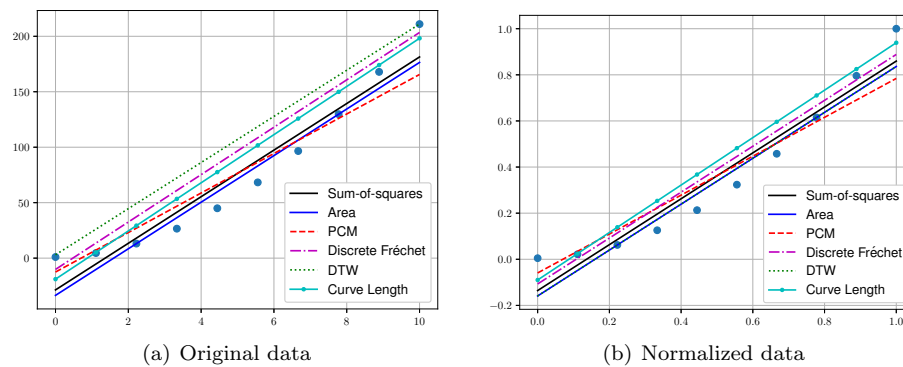

Fig. 8 Results of fitting a line to quadratic data by minimizing different similarity measures. The original data and results are presented in (a), while (b) shows the results with normalized data.

added noise was generated by taking a randomly sampled array from the normal distribution of $\mu = 0.0$ and $\sigma^2 = 0.05$, and then the array was added to the true response. The noise is added only to the dependent variable ($f(x)$), and results in a signal-to-noise ratio (the ratio of the mean to the standard deviation from noise) of 3.33.

Table 1 Parameter bounds and true values for the single load-unload cycle example.

Parameter	Lower bound	True value	Upper bound
β_0	0.0	1.0	10.0
β_1	-10.0	-1.0	10.0
β_2	0.0	1.0	10.0
β_3	0.0	1.0	10.0

The genetic algorithm (GA) was used with the default parameters, except for the maximum number of iterations which were increased from 100 to 200, because the optimizations were still improving after 100 iterations. This optimization problem is more challenging in terms of the number of function evaluations required to find a global optimum, than the previous straight line fits. The GA was used to find the optimal $\boldsymbol{\beta}$ terms that minimize the difference between some guess and the true values. The problem is solved by minimizing either the Area, PCM, discrete Fréchet, DTW, and Curve Length methods. The GA iterations are plotted against the objective function values in Fig. 9. When there isn't noise, the objective values are still improving at 200 iterations, and presumably heading to the known zero objective value. However, when noise is introduced we see that all objective functions stop improving around 100 iterations.

(a) No noise   (b) Added noise
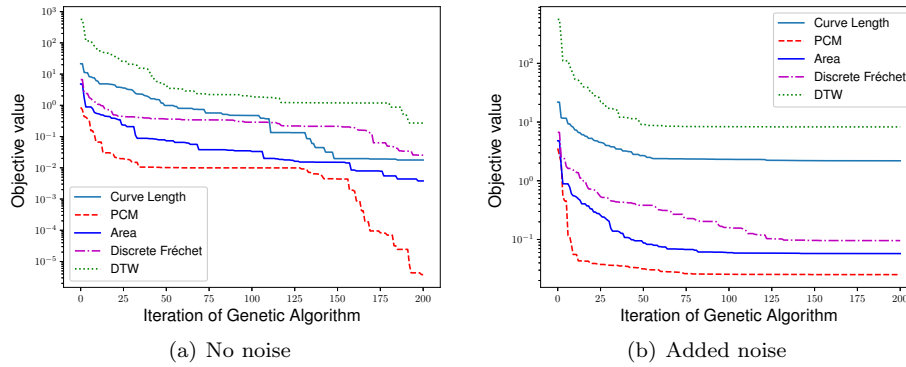
Fig. 9 Plots of the objective values as a function of the iteration of the Genetic Algorithm for the single load-unload cycle example.

All of the objective functions can be minimized to find the true solution. The resulting curves from the best objective functions are shown in Fig. 10. However when noise was present in the data the PCM method struggled, as the optimum objective functions from the noisy data are seen in Fig. 11. DTW and the Area method produced a response that moves through the center of the data points, which is nearly identical to a response by minimizing the sum-of-squares. The line from the sum-of-squares solution is actually covered up by the lines from the DTW and Area methods. The response from the discrete Fréchet distance moves through the data points, but does not remain in the center of the noise. The PCM method

was not capable of finding reasonable parameters with the noisy data. The Curve Length method produced a response that travels on the outer edge of the noise.
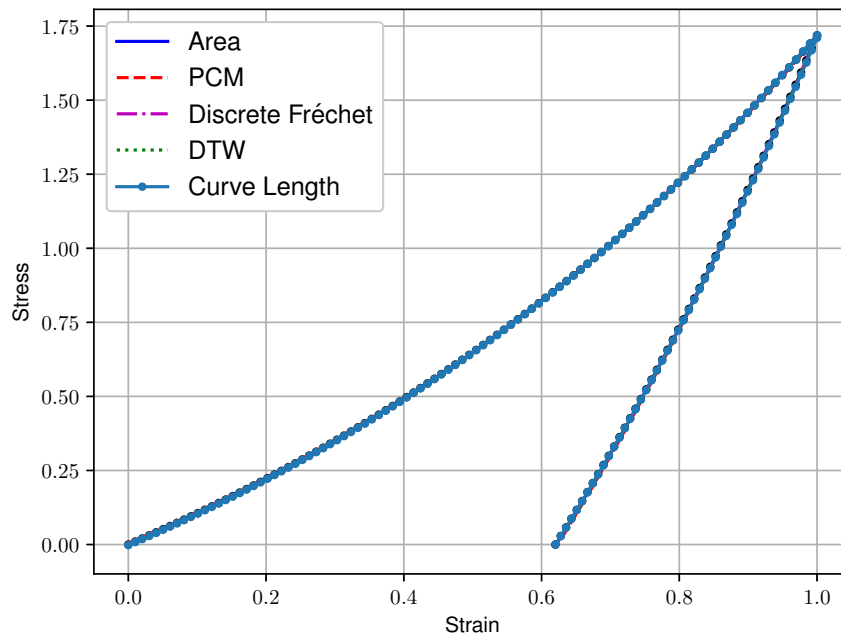

Fig. 10 The curves resulting from the best found objective function values and the original data.

The problem with noise is interesting because it is not possible for any of the objective functions to equal zero. Each optimization found their own best objective function (i.e. minimizing DTW resulted in the best DTW value, minimizing PCM resulted in the best PCM value, etc.). Visually some of these resulting curves (Area, DTW, and sum-of-squares) appear to be better fits than the other objective function values. These fits are just the best according to the minimized objective function. When it was impossible to obtain a perfect fit, the different measures of similarity produced different results. However, each measure of similarity produced nearly identical results when it was possible to obtain a perfect fit.

3.3 Kinematic hardening parameter identification from five cycles

The kinematic hardening parameter identification problem used in Witowski and Stander [27] is revisited to compare the performance of the Area, PCM, discrete Fréchet, DTW, and Curve Length methods. The LS-DYNA material model MAT_125 is calibrated using a single element, and the nine unknown material parameters are determined by matching the response of the LS-DYNA model to five experimental hysteresis tension-compression-tension curves. A single objective function is created by summing the similarity measures between the numerical
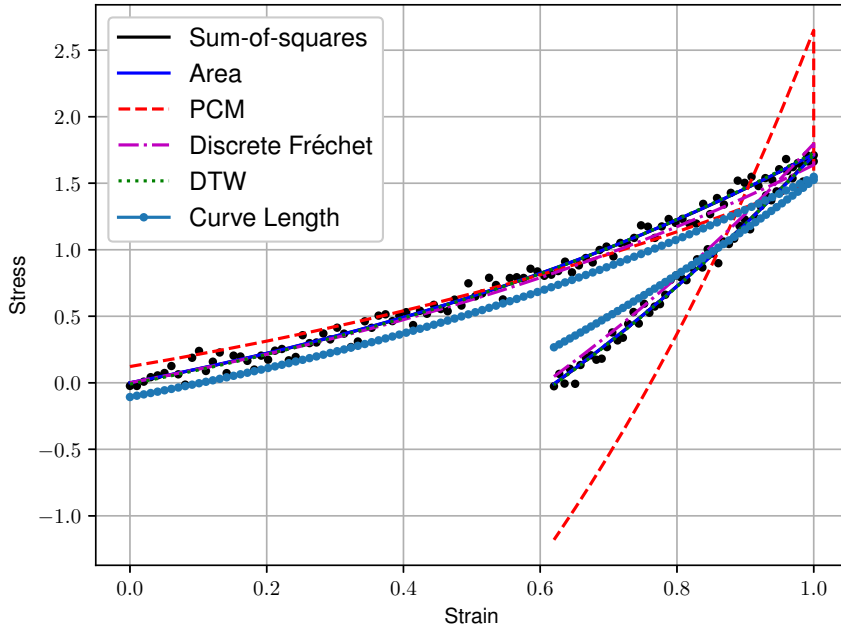
Fig. 11 Curves resulting from the best found objective function values using the noisy data.

model results and the test cycles. Again ten optimizations are run in total, two for each method. The problem is solved with the experimental curves as is, and with artificially added noise.

MAT_125 is based on the kinematic hardening rule developed by Yoshida and Uemori [17], with the addition of allowing the Young's modulus to vary as a function of the effective plastic strain [40]. The manual recommends to use MAT_125 with an implicit FE model when modeling a metal forming process [40]. The material model is not time dependent, thus comparisons of time from the FE model to quasi-static test data may not be relevant.

The parameters are determined in a two part optimization process in an attempt to find the global optimum. First a metamodel (or surrogate) based optimization using the sequential domain reduction (SDRM) technique is run [41]. The SDRM can find reasonable parameters after just a few iterations, though it is not guaranteed to find the true global optimum. The optimum from SDRM is then used as one individual (or the starting point) for a genetic algorithm (GA), in hopes that the GA will find the global optimum. The GA terminates when the relative objective function improvement was less than 0.1% for 100 consecutive iterations. This overall strategy requires a large number of function evaluations on multiple non-linear FE models. If the number of function evaluations is a concern, it may be reasonable to consider using just the SDRM to find a good-enough solution for a fixed number of function evaluations. The optimization bounds are presented in Tab. 2.

The optimizations are performed with and without artificial noise to the test data. The noise was added at random from a normal distribution of $\mu = 0.0, \sigma^2 =$

Table 2 Parameter bounds for the kinematic hardening material model.

Parameter	Lower bound	Upper bound
CB	500	1000
SIGY	450	600
C	90	300
K	10	35
RSAT	250	550
SB	120	400
H	0.5	1.2
C1	0.01	0.1
C2	0.05	0.5

35. The noise is added only to the stress values. The signal-to-noise ratio (consider the mean of the absolute stress value over the standard deviation of the added noise) from the first tension-compression-tension cycle to the last cycle is: 83.1, 105, 117, 127, and 133. These large values suggest that the signal of the hysteresis loop was much stronger than the added noise. It isn't known if this amount of added noise is realistic of an experimental test, but the added noise will provide insight into how the the different similarity measures behave. The added noise represents a case where it is impossible for the numerical model to match the test data exactly. The original test data that was used by Witowski and Stander [27], along with the artificially added noise can be seen in Fig. 12.

The data was first normalized for DTW and Discrete Fréchet measures which were shown sensitive to noise in Fig. 8. The normalization strategy is similar to the PCM method, which sets the stress-strain values of the test curve between zero and one.
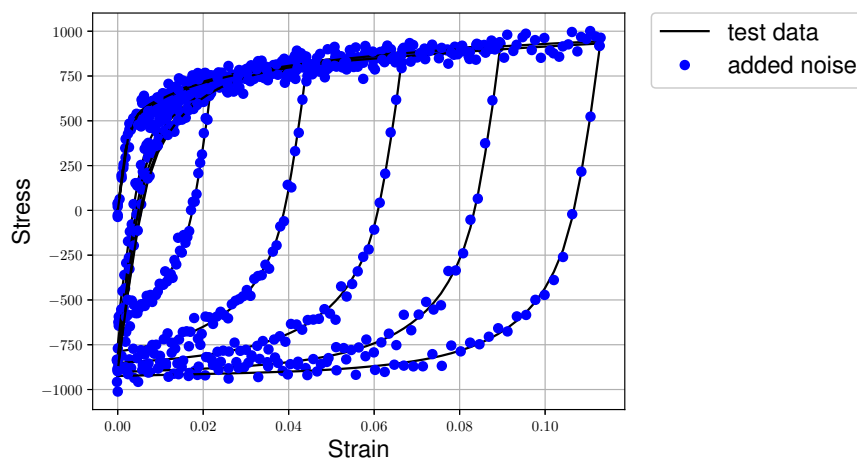
Fig. 12 The five cycles of the original test data as well as the five cycles with artificially added noise.

The numerical model optima responses are seen in Fig. 13, and the results with the added noise in Fig. 14. The PCM method was unable to find reasonable material parameters when noise was added to the test data. Though the results of using Area, discrete Fréchet, DTW, or Curve Length as objective functions appears to produce a stress-strain curve that falls within the noise of the hysteresis data. To view the results of individual hysteresis cycles refer to Appendix C. Qualitatively, the results from the Area, DTW, or Curve Length method appear to match the test data the best. While it appears that the Area, Discrete Fréchet, or DTW methods appear to match the test data with added noised the best.
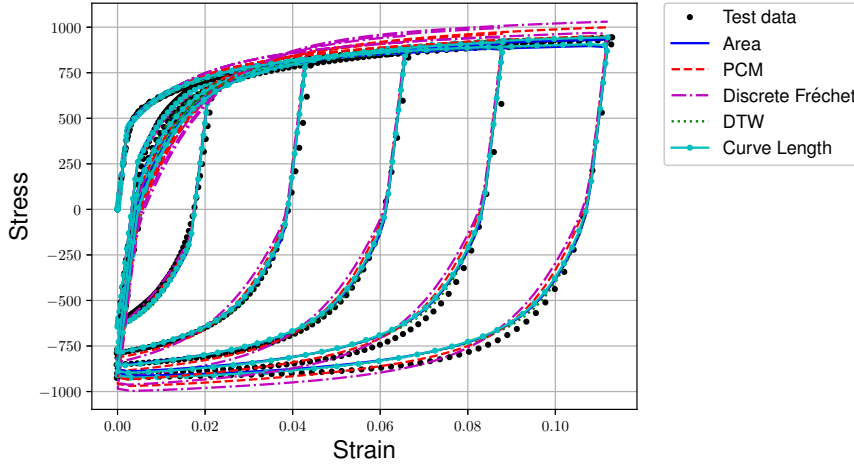

Fig. 13 Material parameter identification optima for MAT‗125 using various measures of similarity.

The parameter values found from each optimization are presented in Tab. 3. Each method recommended different material parameters with a considerable amount of variation. Additionally, variation is present when comparing the results with noise to the results without noise. There is no clear consensus as to what the best set of parameter values should be.

The resulting optima by minimizing one objective function were evaluated by the other measures of similarity, and presented in Tab. 4 and 5. Each global optimization was successful in finding it's own best similarity measure. For the results without noise, the Area, DTW, and Curve Length methods appear to have the most similar objective values.

Line plots between the results of the first SDRM optimization were performed and shown in Appendix B. The line plots indicate whether multiple local optima exist in-between the optima found. Local optima was occasionally found by line plots when considering the cases without added noise (e.g. Fig. 18 a). In general there were fewer local optima (indicated by line plots) when considering the hysteresis loops with artificially added noise.

The results without noise did not find parameters for the MAT‗125 model which result in a zero objective function value. An additional optimization was
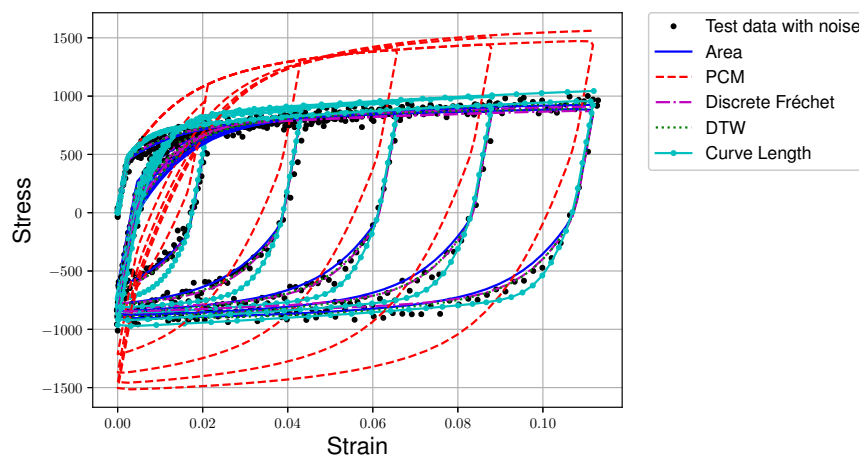
Fig. 14 Material parameter identification optima for MAT_125 using various measures of similarity when noise was artificially added to the test data.

Table 3 Parameters determined from minimizing different objective functions for the kinematic hardening problem. Values at a lower or upper bound do not imply that the similarity measures produce similar material parameters.

Objective function	CB	SIGY	C	K	RSAT	SB	H	C1	C2
without noise									
Area	629	467	160	35	414	196	0.54	0.01	0.12
PCM	687	450	127	24	508	174	0.56	0.01	0.15
Fréchet	763	454	93	23	481	123	0.89	0.02	0.21
DTW	604	451	202	35	493	209	0.50	0.01	0.12
Curve Length	619	451	173	35	389	215	0.51	0.01	0.13
with artificially added noise									
Area	678	450	119	28	328	143	0.50	0.01	0.17
PCM	1000	450	132	35	550	343	1.19	0.01	0.29
Fréchet	720	450	132	11	421	120	0.89	0.02	0.18
DTW	642	451	164	35	407	166	0.50	0.01	0.15
Curve Length	695	472	300	10	550	190	1.19	0.01	0.41

Table 4 Without noise: Objective function values from different optimizations on the kinematic hardening problem. The first column of a row indicates what objective function was minimized by the optimization, while the other columns indicate the other objective function values.

Optimization objective	Method value				
	Area	PCM	Fréchet	DTW	Curve Length
Area	(45.1)	6.3×10^{-3}	0.36	22.5	4.4
PCM	59.7	(3.3×10^{-3})	0.37	27.9	7.5
Fréchet	78.3	4.5×10^{-3}	(0.34)	35.8	10.7
DTW	45.5	5.7×10^{-3}	0.36	(21.7)	4.6
Curve Length	45.5	4.9×10^{-3}	0.36	22.6	(4.3)

Table 5 With added noise: Objective function values from different optimizations on the kinematic hardening problem. The first column of a row indicates which objective function was minimized by the optimization, while the other columns indicate the other objective function values.

Optimization objective	Method value				
	Area	PCM	Fréchet	DTW	Curve Length
Area	(119.0)	1243.8×10^{-3}	0.42	30.2	29.2
PCM	434.1	(832.1×10^{-3})	1.59	176.2	50.3
Fréchet	123.7	1248.3×10^{-3}	(0.40)	30.6	28.7
DTW	120.8	1208.6×10^{-3}	0.44	(28.7)	28.2
Curve Length	150.6	1062.2×10^{-3}	0.59	47.0	(24.9)

run by picking a known set of MAT_125 parameters, and setting the test data to be the result of the FE models from these known parameters. The SDRM optimization produced stress-strain curves that resembled virtual test data. Then when the GA was used to improve upon the SDRM results, it was observed that all objective values were heading to zero. If a perfect fit exist, then any of the measures of similarities can be used to identify the parameters.

A five fold cross validation (CV) study was performed on the kinematic hardening parameter identification problem while trying to determine the differences between similarity measures. This means that the inverse problem was solved using four of the five hysteresis loops, and then validated on the remaining hysteresis loop. The processes was repeated five times such that each loop was used as the validation once. Only the SDRM optimization method was used, because of computational cost restrictions. When these five fold CV results were compared with the initial SDRM results, it was observed that not including a hysteresis loop as data in the inverse problem resulted in material parameters that aren't as good at matching that particular hysteresis loop.

This kinematic hardening parameter identification problem is used as an LS-OPT training example. The data, models, and optimization routines are available upon request.

4 Discussion

The Area, discrete Fréchet, and DTW measures of similarity are similar to traditionally statistical measures of similarity between curves. The discrete Fréchet distance is similar to the maximum error, as both methods (when minimized) are sensitive to outliers. Despite different rationale, the Area and DTW methods are similar to the sum-of-errors (or mean absolute deviation). The Area and DTW methods could be modified to produce analogous results to the sum-of-squares solution. This could be accomplished by squaring the distances in DTW, or by squaring the areas in the Area method. Together these methods are similar to the standard L1 norm, L2 norm, and L-infinity norm with an advantage of being particularly useful for identifying unique hysteresis loops.

It is worthwhile to note that all of the similarity measures would return an objective function value of zero for the exact $\boldsymbol{\beta}$ parameters when considering noiseless

data. For perfect global optimization, there will be a non-zero residual for an imperfect model. There is always the potential that an imperfect model could be be improved with a better physical understanding of the problem (e.g. selecting a better material model, or more appropriate FE model). When the noisy data is considered there will always be a non-zero objective function value. In all examples, the PCM method was more sensitive to the noise than the other methods. The PCM method is known to be sensitive to noise, thus the LS-OPT manual recommends to use a noise filter to pre-process the curve before using PCM. If it was possible to completely filter out the noise, then the results without noise would be identical to the results with noise for all problems.

The discrete Fréchet distance and DTW produced different straight lines when considering the normalized and original quadratic data, as shown in Fig. 8. This was a result of the algorithms focusing on removing the distance in the variable that was an order of magnitude larger than the other variable. It is recommended to first normalize stress-strain responses when applying discrete Fréchet distance and DTW as stress can be orders of magnitude larger than strain. It is worthwhile to mention that normalization is built into the PCM and Curve Length methods by default.

Using partial matching algorithms, such as PCM, may sometimes be preferable to the other measures of similarity. For instance consider a case where the numerical model was only replicating the loading stage of a hysteresis loop. In this case, PCM is the only method that can be applied to find a partial match of just the initial tension section of the hysteresis loop shown in Fig. 15. The PCM is the only measure of similarity in this paper that would return a zero value for this partial mapping. Tormene et al. [42] proposed a partial matching DTW strategy that is available in the R *dtw* package. Partial matching DTW was not covered in this study, but it may be of interest for future work.

Each measure of similarity presented has its own advantages when being used for parameter identification. The PCM method is capable of matching partial responses. The Discrete Fréchet distance would be useful at reducing the maximum error at any location of two curves. The Area and Curve Length methods appear to have a smoother design space than the other measures when comparing the line plots in Appendix A. It may be preferable to use gradient based optimizations on smooth objective functions which would have fewer local minima than non-smooth objective functions. A qualitative comparison of the objective functions is presented in Tab. 6.

Table 6 A qualitative comparison of the objective functions covered in this work.

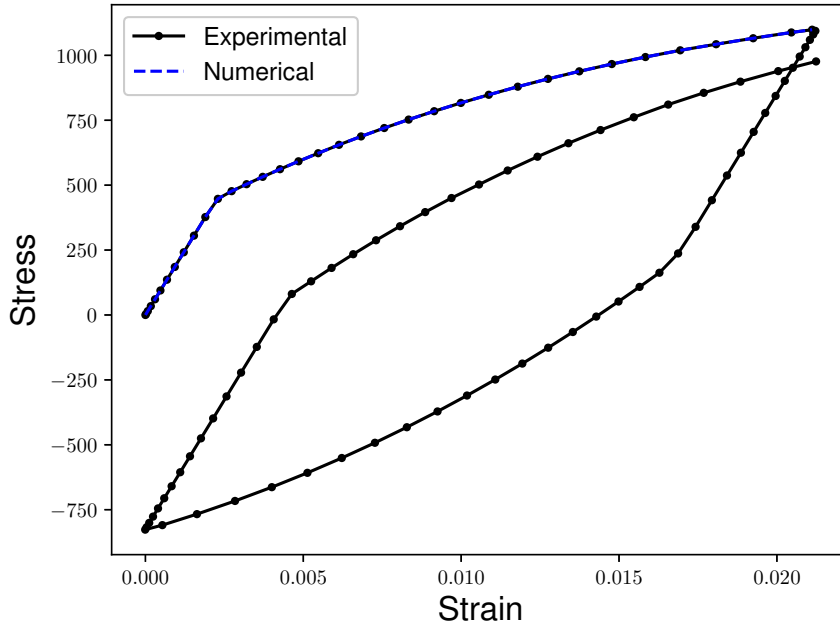| Objective function	Partial matching	Resistance to noise	Resistance to outliers	Function shape
Area	no	good	good	smooth
PCM	yes	poor	poor	non-smooth
Fréchet	no	fair	poor	non-smooth
DTW	see [42]	good	good	less smooth
Curve Length	no	fair	good	smooth

Fig. 15 Partial mapping example where the PCM objective function value is zero between numerical and experimental curve.

Consider a problem where the data is perfect, meaning that there is no noise and all data points are trusted. All five similarity measures presented will return zero for a numerical model that matched the data exactly. Ideally this would represent a global optimum for the numerical model. If the numerical model was unable to replicate the behavior from just one experimental data point, then each similarity measure may have a unique global optimum recommending a different set of model parameters. The differences in identified parameters would be the result of the interpretation of each similarity measure. A comparison of the measures of similarity for imperfect fits was best illustrated in section 3.1, with Figs. 7 and 8. This is reasonable motivation to consider multiple similarity measures, as often it is impossible for numerical models to match experimental data exactly. For example, it could be impossible to obtain a perfect match if the numerical model inadequately captured the physics of an experimental response, or if there are errors associated with the experimental response.

5 Conclusion

Five different measures of similarity between two curves are presented. The PCM, discrete Fréchet, DTW, and Curve Length measures are from literature. Additionally, a new algorithm is presented to approximate the Area between two curves. These five methods offer advantages over traditional sum-of-square methods, because they don't require the numerical model to be aligned with the experimental

data. Additionally they may work particularly well with hysteresis loops, load-unload cycles, or tension-compression tests. These similarity measures can be considered as alternatives to error formulations based on the sum-of-squares, as they help quantify the quality of fit between an experimental and numerical curve. These quantities can be minimized in an inverse analysis to aid in the identification of material parameters. Note that this work assumes that the curves are in a particular time-series order from an initial point to a final point.

When there is no noise present in the data, the results of minimizing either the Area, PCM, discrete Fréchet, DTW, or Curve Length similarity measures produce a reasonable solution. If a perfect fit is possible, any single similarity measure can be used to find the parameters that determine the perfect match. If it is impossible for the numerical model to match the experiment exactly, each method may yield a different solution due to the different physical interpretation of each method. For practical problems it is often impossible to match the experimental data exactly. In these cases, it would be useful to have the best set of parameters from multiple similarity measures. Differences between sets of material parameters may provide an indication of the uncertainty associated with each parameter.

A Algorithm to calculate area between two curves

The area of any simple (non self intersecting) quadrilateral can be expressed by Gauss's area formula (also known as the shoelace formula). Gauss's area formula for a simple quadrilateral is

$$A = \frac{1}{2}\left| x_1 y_2 + x_2 y_3 + x_3 y_4 + x_4 y_1 - x_2 y_1 - x_3 y_2 - x_4 y_3 - x_1 y_4 \right| \qquad (3)$$

where A is the area and (x_i, y_i) represents the vertices of the quadrilateral. It is worthwhile to note that any complex quadrilateral can become a simple quadrilateral by rearranging the order of the vertices.
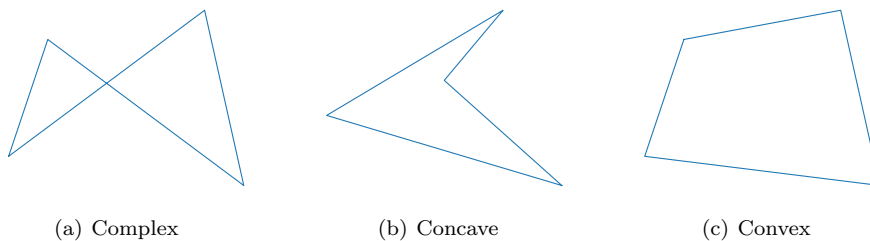

(a) Complex   (b) Concave   (c) Convex

Fig. 16 Examples of complex and simple quadrilaterals. A simple quadrilateral can be either concave or convex.

The interior angles of a quadrilateral can be used to detect whether a quadrilateral is simple or complex. Any simple quadrilateral will have a sum of interior angles that add up to $360°$. If all interior angles are less than $180°$, the simple quadrilateral is said to be convex. However if one interior angle is greater than $180°$, the simple quadrilateral is said to be concave. The interior angles of complex quadrilaterals will add up to $720°$. An example of a complex, concave, and convex quadrilaterals are shown in Fig. 16.

The change of sign of cross products can be used to detect if a quadrilateral is complex (as an interpretation of the interior angles). Let's consider an arbitrary quadrilateral represented
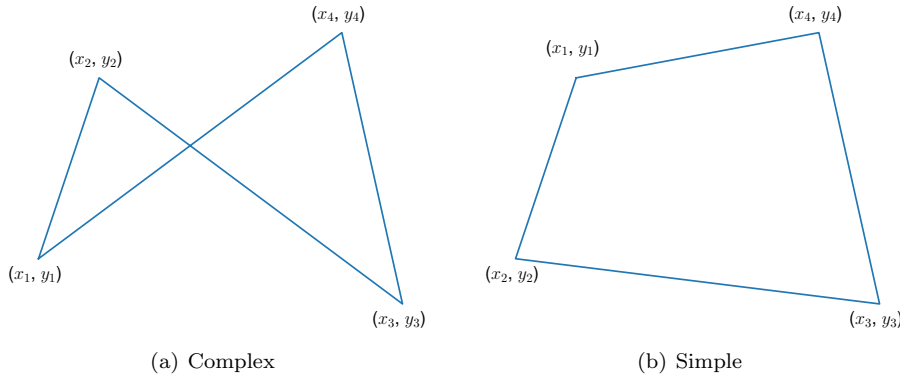
(a) Complex

(b) Simple

Fig. 17 By swapping the vertices of (x_1, y_1) with (x_2, y_2), the complex quadrilateral of (a) becomes the simple quadrilateral in (b).

by the following vectors:

$$\boldsymbol{AB} = \langle x_2 - x_1, y_2 - y_1 \rangle \tag{4}$$
$$\boldsymbol{BC} = \langle x_3 - x_2, y_3 - y_2 \rangle \tag{5}$$
$$\boldsymbol{CD} = \langle x_4 - x_3, y_4, -y_3 \rangle \tag{6}$$
$$\boldsymbol{DA} = \langle x_1 - x_4, y_1 - y_4 \rangle \tag{7}$$

The sign of the following cross products dictates whether a quadrilateral is self intersecting or not.

$$\boldsymbol{AB} \times \boldsymbol{BC} \tag{8}$$
$$\boldsymbol{BC} \times \boldsymbol{CD} \tag{9}$$
$$\boldsymbol{CD} \times \boldsymbol{DA} \tag{10}$$
$$\boldsymbol{DA} \times \boldsymbol{AB} \tag{11}$$

A complex quadrilateral exists if and only if two of the above cross products are negative and the other two are positive. A simple quadrilateral will have at least three of the same sign cross products. The vertices of a complex quadrilateral can be used to create a simple quadrilateral simply by rearranging the order as shown in Fig. 17.

A pseudocode algorithm to compute the effective area between two curves is presented as Algorithm 1. The algorithm first ensures that the two curves have the same number of data points. If not, points are added to the curve with fewer points. The total number of quadrilaterals created will be one less than the number of data points. Two consecutive points are taken from each curve, acting as the vertices of the quadrilateral. Note that the order of the data points which represent the curve is important. The first quadrilateral uses the first and second data point from each curve, the second quadrilateral uses the second and third data point from each curve and so forth. Each quadrilateral is then determined to be either simple or complex. If the quadrilateral is complex, the vertices are reordered until the quadrilateral becomes simple. The area of each simple quadrilateral is calculated using the Gauss area formula, and all quadrilateral areas are summed to give an effective area between curves.

B Line plot for kinematic hardening problem

Line plots were performed in between data points of the kinematic hardening problem to visualize the design space with different similarity measures. All objective function values were

---

Algorithm 1: Compute the effective area between curveA and curveB.

---

1 function areaBetweenCurves (curveA, curveB);
   Input : Data of curveA and curveB.
   Output: Area between curveA and curveB.
2 # the length() function returns the number of data points
3 **if** $length(curveA) < length(curveB)$ **then**
4 | A = curveA;
5 | B = curveB;
6 **else**
7 | B = curveA;
8 | A = curveB;
9 **end**
10 **while** $length(A) < length(B)$ **do**
11 | Compute distance between every two consecutive points of A;
12 | Find the two points that generate the max distance;
13 | Create a point that bisects these two points;
14 | Add the bisect point to A in between the two points;
15 **end**
16 n = length(A) -1; # compute the number of quadrilaterals;
17 areas = zeros (n); # initiate zeros array for areas;
18 **for** $i = 1$ to n **do**
19 | # Assemble quadrilateral;
20 | quad = [A[i], A[i+1], B[i+1], B[i]];
21 | **if** $quad is not simple$ **then**
22 | | Rearrange the order of vertices until quad is simple;
23 | **end**
24 | # Calculate the Gauss/shoelace area of the quadrilateral;
25 | areas[i] = gaussArea(quad);
26 **end**
27 # Return the summation of quadrilateral areas;
28 return sum(areas);

---

normalized using

$$z_i = \frac{x_i - \min(\boldsymbol{x})}{\max(\boldsymbol{x}) - \min(\boldsymbol{x})} \tag{12}$$

such that zero is the best found objective function, and one is the worst. The line plots without noise are presented in Fig. 18, and the line plots with noise are presented in Fig. 19. The line plots help to illustrate the state of the design space (for each measure of similarity) between the optima found. Additionally it appears that the Area and Curve Length methods produced smoother design spaces than the PCM and Discrete Fréchet methods. The line plots were calculated from the results of the first SDRM optimization result, and sometimes display a local optimum that the SDRM failed to find.

C Kinematic hardening results

It is difficult to recognize the differences between similarity measures for the kinematic hardening parameter identification from section 3.3. This appendix section shows the results from section 3.3 for the individual hysteresis loops. The results of the hysteresis curve from the parameter identification can be seen in Figs. 20- 24, and the results with noise in Figs. 25- 29.

References

1. Mary C Boyce and Ellen M Arruda. Constitutive Models of Rubber Elasticity: A Review. *Rubber Chemistry and Technology*, 73(3):504–523, 2000. doi: 10.5254/1.3547602. URL `https://doi.org/10.5254/1.3547602`.
2. M Grédiac, F Pierron, and A Vautrin. The Iosipescu in-plane shear test applied to composites: A new approach based on displacement field processing. *Composites Science and Technology*, 51(3):409–417, 1994. ISSN 0266-3538. doi: https://doi.org/ 10.1016/0266-3538(94)90109-0. URL `http://www.sciencedirect.com/science/article/pii/0266353894901090`.
3. M Grédiac, F Pierron, S Avril, and E Toussaint. The Virtual Fields Method for Extracting Constitutive Parameters From Full-Field Measurements: a Review. *Strain*, 42(4):233–253, 2006. ISSN 1475-1305. doi: 10.1111/j.1475-1305.2006.tb01504.x. URL `http://dx.doi.org/10.1111/j.1475-1305.2006.tb01504.x`.
4. D S Schnur and Nicholas Zabaras. An inverse method for determining elastic material properties and a material interface. *International Journal for Numerical Methods in Engineering*, 33(10):2039–2057, 1992. ISSN 1097-0207. doi: 10.1002/nme.1620331004. URL `http://dx.doi.org/10.1002/nme.1620331004`.
5. Georges Lovato, F Moret, P Le Gallo, Georges Cailletaud, and Philippe Pilvin. Determination of brazed joint constitutive law by inverse method. *Le Journal de Physique IV*, 3 (C7):C7—-1135, 1993.
6. J C Gelin and O Ghouati. An inverse method for determining viscoplastic properties of aluminium alloys. *Journal of Materials Processing Technology*, 45(1):435–440, 1994. ISSN 0924-0136. doi: https://doi.org/10.1016/0924-0136(94)90378-6. URL `http://www.sciencedirect.com/science/article/pii/0924013694903786`.
7. Ole Sigmund. Materials with prescribed constitutive parameters: An inverse homogenization problem. *International Journal of Solids and Structures*, 31(17):2313–2329, 1994. ISSN 0020-7683. doi: https://doi.org/10.1016/0020-7683(94)90154-6. URL `http://www.sciencedirect.com/science/article/pii/0020768394901546`.
8. G Cailletaud and Philippe Pilvin. Identification and inverse problems related to material behaviour. *Inverse problems in engineering mechanics*, 1:79–86, 1994.
9. D Lederer, H Igarashi, A Kost, and T Honma. On the parameter identification and application of the Jiles-Atherton hysteresis model for numerical modelling of measured characteristics, 1999.
10. H Haddadi, S Bouvier, M Banu, C Maier, and C Teodosiu. Towards an accurate description of the anisotropic behaviour of sheet metals under large plastic deformations: Modelling, numerical analysis and identification. *International Journal of Plasticity*, 22(12):2226–2271, 2006. ISSN 0749-6419. doi: 10.1016/j.ijplas.2006.03.010. URL `http://www.sciencedirect.com/science/article/pii/S0749641906000386`.
11. Per-Anders Eggertsen and Kjell Mattiasson. On the identification of kinematic hardening material parameters for accurate springback predictions. *International Journal of Material Forming*, 4(2):103–120, 2011. ISSN 1960-6214. doi: 10.1007/s12289-010-1014-7. URL `http://dx.doi.org/10.1007/s12289-010-1014-7`.
12. T Harth, S Schwan, J Lehn, and F G Kollmann. Identification of material parameters for inelastic constitutive models: statistical analysis and design of experiments. *International Journal of Plasticity*, 20(8):1403–1440, 2004. ISSN 0749-6419. doi: http://dx.doi.org/10.1016/j.ijplas.2003.11.001. URL `http://www.sciencedirect.com/science/article/pii/S0749641903001566`.
13. M Rabahallah, T Balan, S Bouvier, B Bacroix, F Barlat, K Chung, and C Teodosiu. Parameter identification of advanced plastic strain rate potentials and impact on plastic anisotropy prediction. *International Journal of Plasticity*, 25(3):491–512, 2009. ISSN 0749-6419. doi: http://dx.doi.org/10.1016/j.ijplas.2008.03.006. URL `http://www.sciencedirect.com/science/article/pii/S0749641908000478`.
14. N Souto, A Andrade-Campos, and S Thuillier. Material parameter identification within an integrated methodology considering anisotropy, hardening and rupture. *Journal of Materials Processing Technology*, 220:157–172, 2015.

15. F Yoshida, M Urabe, R Hino, and V V Toropov. Inverse approach to identification of material parameters of cyclic elasto-plasticity for component layers of a bimetallic sheet. *International Journal of Plasticity*, 19(12):2149–2170, 2003. ISSN 0749-6419. doi: http://dx.doi.org/10.1016/S0749-6419(03)00063-9. URL `http://www.sciencedirect.com/science/article/pii/S0749641903000639`.

16. R De-Carvalho, R A F Valente, and A Andrade-Campos. On the Objective Function Evaluation in Parameter Identification of Material Constitutive Models - Single-point or FE Analysis. *International Journal of Material Forming*, 3(1):33–36, 2010. ISSN 1960-6214. doi: 10.1007/s12289-010-0700-9. URL `http://dx.doi.org/10.1007/s12289-010-0700-9`.

17. Fusahito Yoshida and Takeshi Uemori. A model of large-strain cyclic plasticity describing the Bauschinger effect and workhardening stagnation. *International Journal of Plasticity*, 18(5):661–686, 2002. ISSN 0749-6419. doi: http://dx.doi.org/10.1016/S0749-6419(01)00050-X. URL `http://www.sciencedirect.com/science/article/pii/S074964190100050X`.

18. Daeyong Kim, Frédéric Barlat, Salima Bouvier, Meziane Rabahallah, Tudor Balan, and Kwansoo Chung. Non-quadratic anisotropic potentials based on linear transformation of plastic strain rate. *International Journal of Plasticity*, 23(8):1380–1399, 2007. ISSN 0749-6419. doi: http://dx.doi.org/10.1016/j.ijplas.2007.01.006. URL `http://www.sciencedirect.com/science/article/pii/S0749641907000071`.

19. Maxime Gruber, Nadhir Lebaal, Sebastien Roth, Nizar Harb, Peter Sterionow, and François Peyraut. Parameter identification of hardening laws for bulk metal forming using experimental and numerical approach. *International Journal of Material Forming*, 9(1):21–33, 2016. ISSN 1960-6214. doi: 10.1007/s12289-014-1196-5. URL `http://dx.doi.org/10.1007/s12289-014-1196-5`.

20. Hamad ul Hassan, Fawad Maqbool, Alper Güner, Alexander Hartmaier, Nooman Ben Khalifa, and A Erman Tekkaya. Springback prediction and reduction in deep drawing under influence of unloading modulus degradation. *International Journal of Material Forming*, 9(5):619–633, nov 2016. ISSN 1960-6214. doi: 10.1007/s12289-015-1248-5. URL `https://doi.org/10.1007/s12289-015-1248-5`.

21. E Markiewicz and B Langrand. Characterisation and Parameters Identification of Materials Constitutive and Damage Models: From Normalised Direct Approach to Most Advanced Inverse Problem Resolution. *Procedia Engineering*, 173:33–40, 2017. ISSN 1877-7058. doi: https://doi.org/10.1016/j.proeng.2016.12.016. URL `http://www.sciencedirect.com/science/article/pii/S1877705816344071`.

22. A Andrade-Campos, R De-Carvalho, and R A F Valente. Novel criteria for determination of material model parameters. *International Journal of Mechanical Sciences*, 54(1):294–305, 2012. ISSN 0020-7403. doi: https://doi.org/10.1016/j.ijmecsci.2011.11.010. URL `http://www.sciencedirect.com/science/article/pii/S0020740311002451`.

23. P A L S Martins, R M Natal Jorge, and A J M Ferreira. A Comparative Study of Several Material Models for Prediction of Hyperelastic Properties: Application to Silicone-Rubber and Soft Tissues. *Strain*, 42(3):135–147, 2006. ISSN 1475-1305. doi: 10.1111/j.1475-1305.2006.00257.x. URL `http://dx.doi.org/10.1111/j.1475-1305.2006.00257.x`.

24. O T Bruhns and D K Anding. On the simultaneous estimation of model parameters used in constitutive laws for inelastic material behaviour. *International Journal of Plasticity*, 15(12):1311–1340, 1999. ISSN 0749-6419. doi: http://dx.doi.org/10.1016/S0749-6419(99)00046-7. URL `http://www.sciencedirect.com/science/article/pii/S0749641999000467`.

25. D H Wolpert and W G Macready. No free lunch theorems for optimization. *IEEE Transactions on Evolutionary Computation*, 1(1):67–82, apr 1997. ISSN 1089-778X. doi: 10.1109/4235.585893.

26. N. Stander, W. Roux, T. Goel, T. Eggleston, and K. Craig. *LS-OPT ® User's Manual - A Design Optimization and Probabilistic Analysis Tool*. 2015.

27. Katharina Witowski and Nielen Stander. Parameter Identification of Hysteretic Models Using Partial Curve Mapping. *12th AIAA Aviation Technology, Integration, and Operations (ATIO) Conference and 14th AIAA/ISSMO Multidisciplinary Analysis and Optimization Conference*, sep 2012. doi: doi:10.2514/6.2012-5580.

28. Martin P Venter and Gerhard Venter. Simple implementation of plain woven polypropylene fabric. *Journal of Industrial Textiles*, aug 2016. doi: 10.1177/1528083716665627.

29. M Maurice Fréchet. Sur quelques points du calcul fonctionnel. *Rendiconti del Circolo Matematico di Palermo (1884-1940)*, 22(1):1–72, 1906.

30. Thomas Eiter and Heikki Mannila. Computing discrete Fréchet distance. Technical report, 1994.
31. Anne Driemel, Sariel Har-Peled, and Carola Wenk. Approximating the Fréchet Distance for Realistic Curves in Near Linear Time. *Discrete & Computational Geometry*, 48(1): 94–127, 2012. ISSN 1432-0444. doi: 10.1007/s00454-012-9402-z. URL `http://dx.doi.org/10.1007/s00454-012-9402-z`.
32. K Bringmann. Why Walking the Dog Takes Time: Frechet Distance Has No Strongly Subquadratic Algorithms Unless SETH Fails, 2014.
33. Sean L Seyler, Avishek Kumar, M F Thorpe, and Oliver Beckstein. Path Similarity Analysis: A Method for Quantifying Macromolecular Pathways. *PLOS Computational Biology*, 11(10):1–37, 2015. doi: 10.1371/journal.pcbi.1004568. URL `https://doi.org/10.1371/journal.pcbi.1004568`.
34. Helmut Alt and Michael Godau. Computing the Fréchet Distance Between Two Polygonal Curves. *International Journal of Computational Geometry & Applications*, 05(01n02):75–91, 1995. doi: 10.1142/S0218195995000064.
35. Donald J Berndt and James Clifford. Using Dynamic Time Warping to Find Patterns in Time Series. In *Proceedings of the 3rd International Conference on Knowledge Discovery and Data Mining*, AAAIWS'94, pages 359–370. AAAI Press, 1994. URL `http://dl.acm.org/citation.cfm?id=3000850.3000887`.
36. François Petitjean, Alain Ketterlin, and Pierre Gançarski. A global averaging method for dynamic time warping, with applications to clustering. *Pattern Recognition*, 44(3): 678–693, 2011. ISSN 0031-3203. doi: https://doi.org/10.1016/j.patcog.2010.09.013. URL `http://www.sciencedirect.com/science/article/pii/S003132031000453X`.
37. Toni Giorgino. Computing and Visualizing Dynamic Time Warping Alignments in R: The dtw Package. *Journal of Statistical Software; Vol 1, Issue 7 (2009)*, aug 2009. URL `http://dx.doi.org/10.18637/jss.v031.i07`.
38. Stan Salvador and Philip Chan. Toward Accurate Dynamic Time Warping in Linear Time and Space. *Intell. Data Anal.*, 11(5):561–580, oct 2007. ISSN 1088-467X. URL `http://dl.acm.org/citation.cfm?id=1367985.1367993`.
39. J Cao and J Lin. A study on formulation of objective functions for determining material models. *International Journal of Mechanical Sciences*, 50(2):193–204, 2008. ISSN 0020-7403. doi: https://doi.org/10.1016/j.ijmecsci.2007.07.003. URL `http://www.sciencedirect.com/science/article/pii/S0020740307001178`.
40. Livermore Software Technology Corporation. *MAT_KINEMATIC_HARDENING_TRANSVERSELY_ANISOTROPIC. In *LS-DYNA Keyword User's Manual Volume II Material Models*, pages 635–646. 2016.
41. Nielen Stander and K J Craig. On the robustness of a simple domain reduction scheme for simulation-based optimization. *Engineering Computations*, 19(4):431–450, 2002. doi: 10.1108/02644400210430190.
42. Paolo Tormene, Toni Giorgino, Silvana Quaglini, and Mario Stefanelli. Matching incomplete time series with dynamic time warping: an algorithm and an application to post-stroke rehabilitation. *Artificial Intelligence in Medicine*, 45(1):11–34, 2009. ISSN 0933-3657. doi: https://doi.org/10.1016/j.artmed.2008.11.007. URL `http://www.sciencedirect.com/science/article/pii/S0933365708001772`.
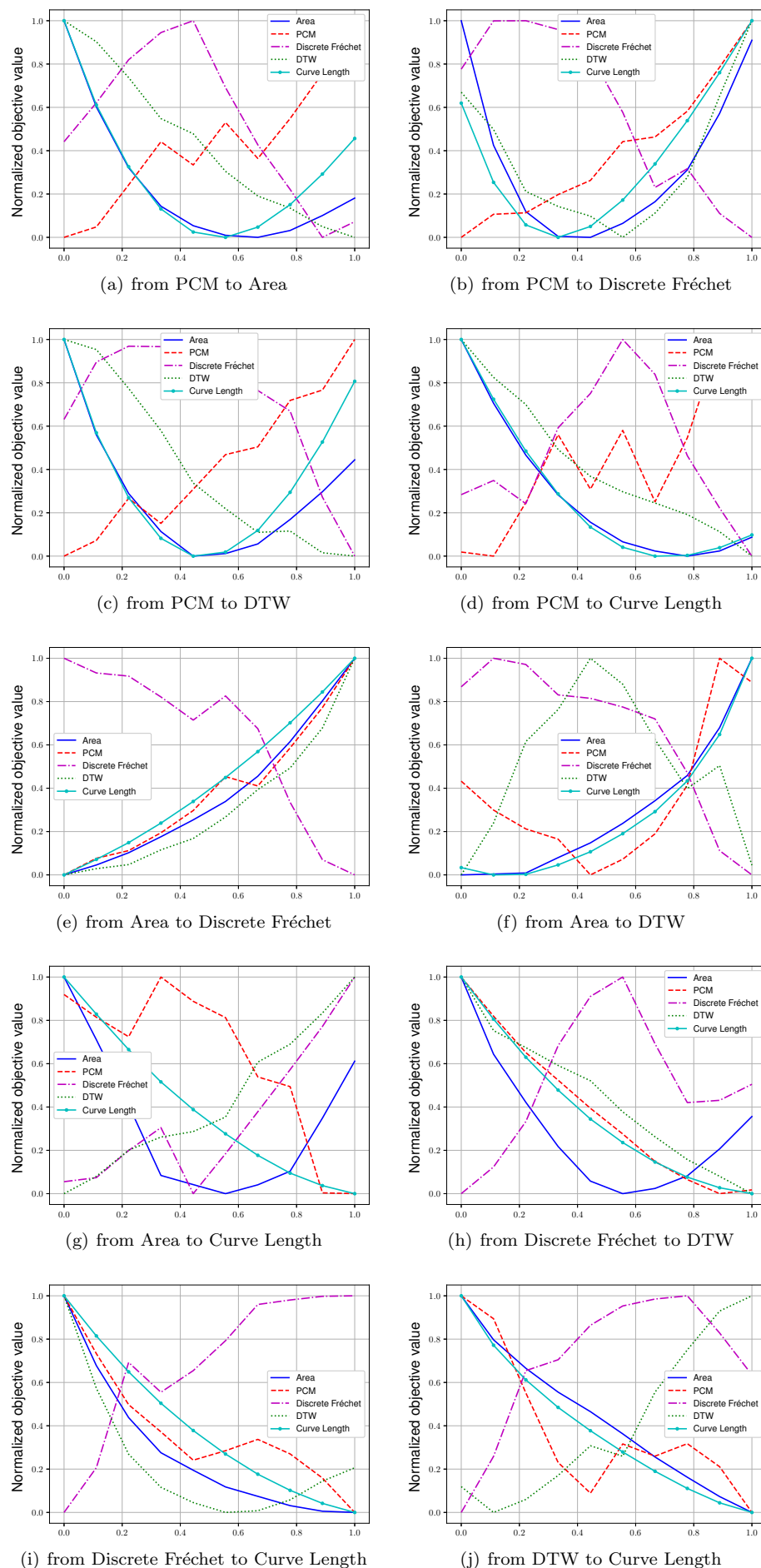
(a) from PCM to Area

(b) from PCM to Discrete Fréchet

(c) from PCM to DTW

(d) from PCM to Curve Length

(e) from Area to Discrete Fréchet

(f) from Area to DTW

(g) from Area to Curve Length

(h) from Discrete Fréchet to DTW

(i) from Discrete Fréchet to Curve Length

(j) from DTW to Curve Length

Fig. 18 Without noise: Line plot with normalized objective values from one objective optimum to another objective optimum.

(a) from PCM to Area

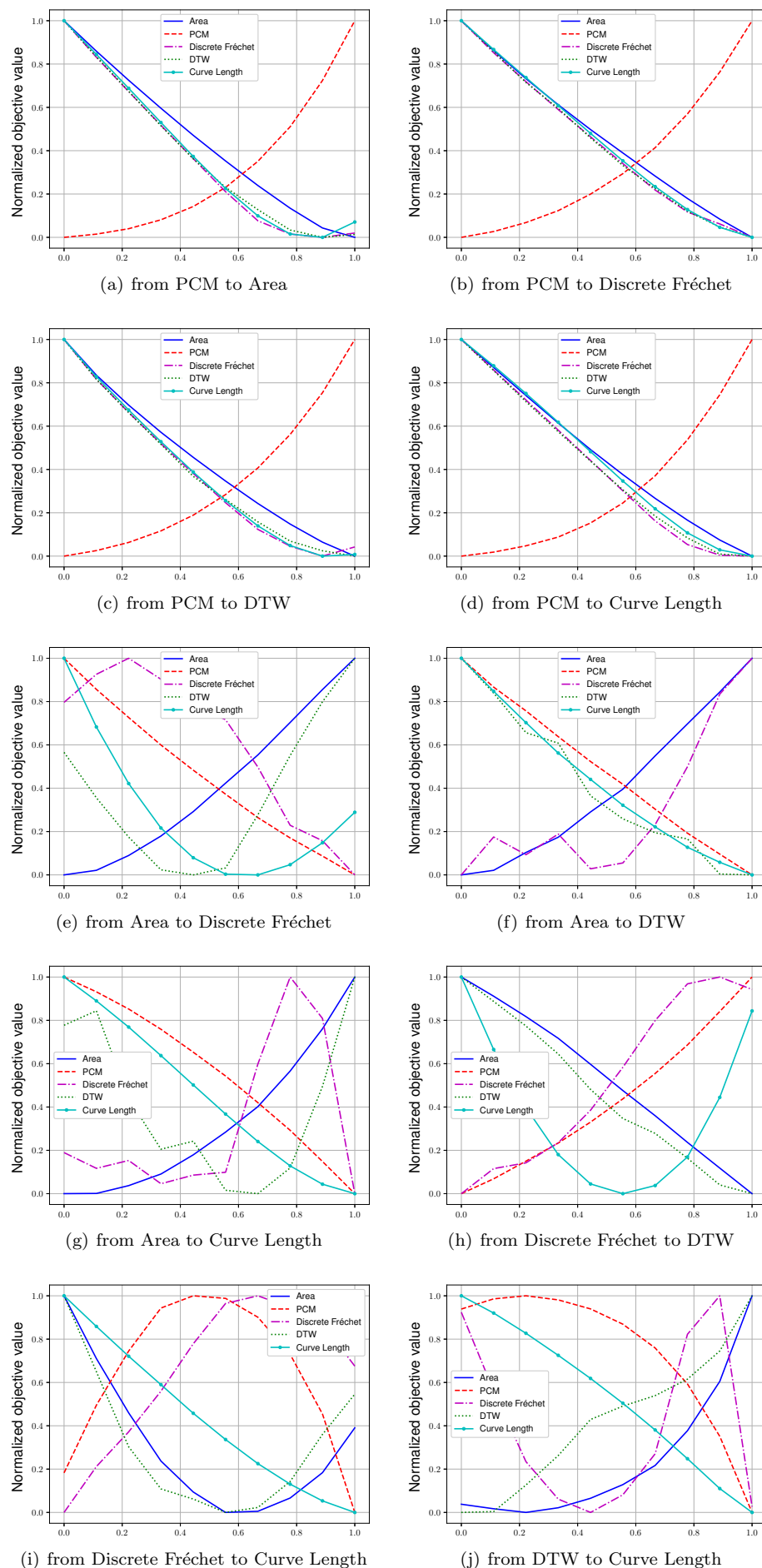(b) from PCM to Discrete Fréchet

(c) from PCM to DTW

(d) from PCM to Curve Length

(e) from Area to Discrete Fréchet

(f) from Area to DTW

(g) from Area to Curve Length

(h) from Discrete Fréchet to DTW

(i) from Discrete Fréchet to Curve Length

(j) from DTW to Curve Length

Fig. 19 With noise: Line plot with normalized objective values from one objective optimum to another objective optimum.

(a) first cycle   (b) second cycle   (c) third cycle

(d) fourth cycle   (e) fifth cycle
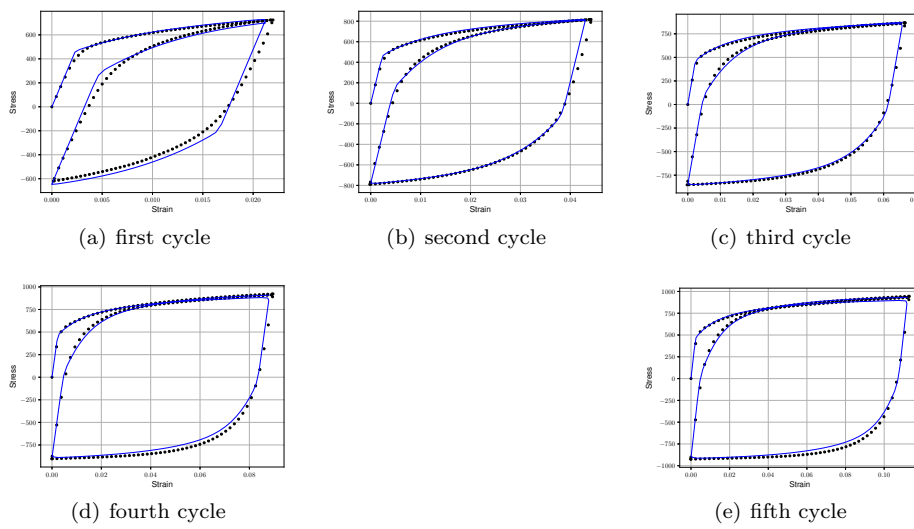
Fig. 20 Area results for kinematic hardening parameter identification.

(a) first cycle   (b) second cycle   (c) third cycle

(d) fourth cycle   (e) fifth cycle
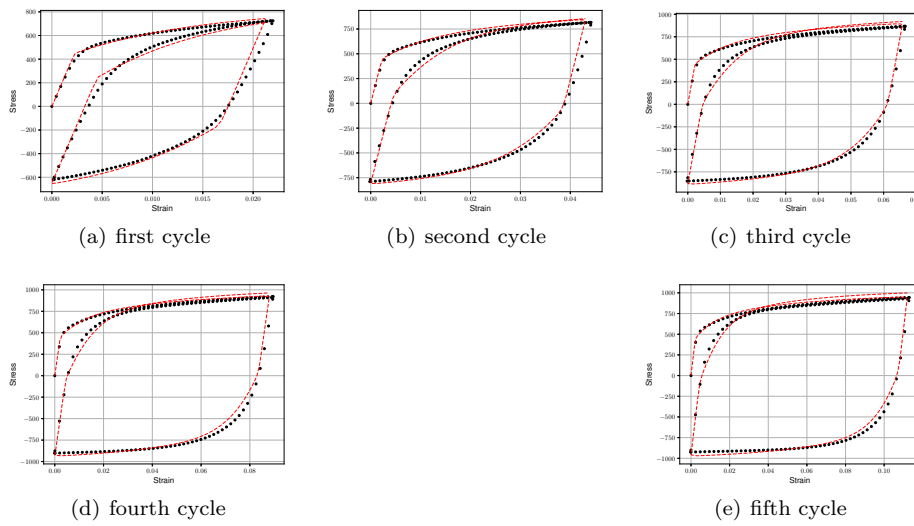
Fig. 21 PCM results for kinematic hardening parameter identification.

(a) first cycle   (b) second cycle   (c) third cycle

(d) fourth cycle   (e) fifth cycle
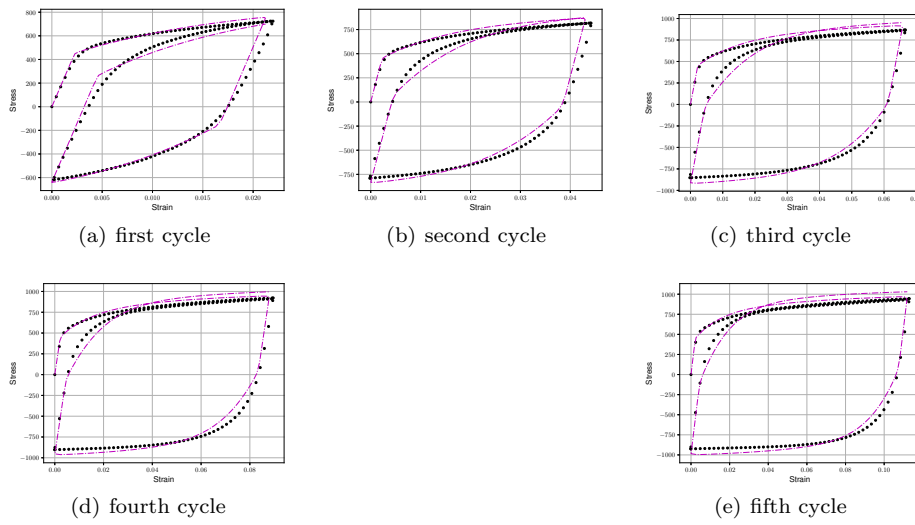
Fig. 22 Discrete Fréchet results for kinematic hardening parameter identification.

(a) first cycle   (b) second cycle   (c) third cycle

(d) fourth cycle   (e) fifth cycle
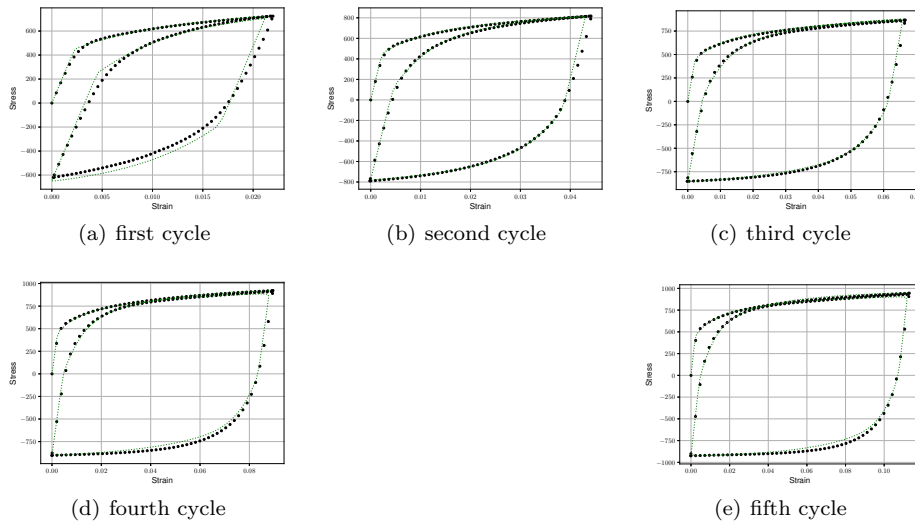
Fig. 23 DTW results for kinematic hardening parameter identification.

(a) first cycle   (b) second cycle   (c) third cycle

(d) fourth cycle   (e) fifth cycle
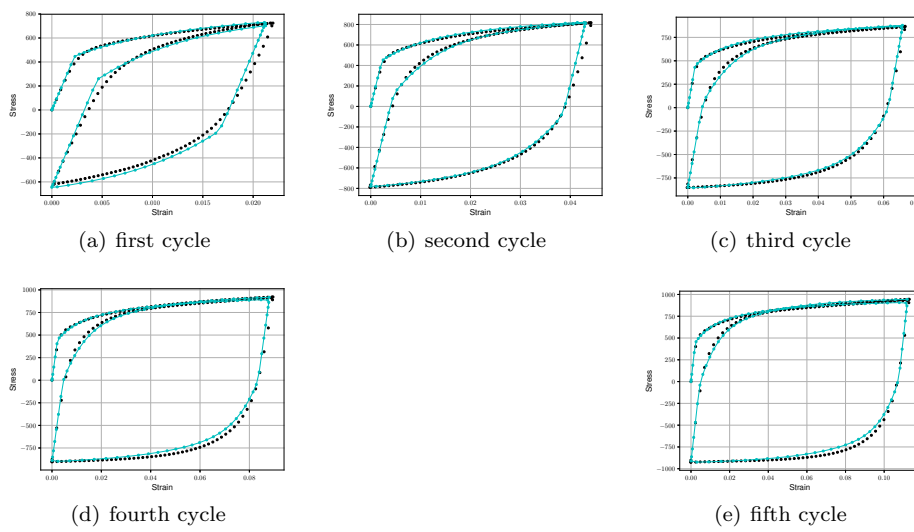
Fig. 24 Curve Length results for kinematic hardening parameter identification.

(a) first cycle   (b) second cycle   (c) third cycle

(d) fourth cycle   (e) fifth cycle
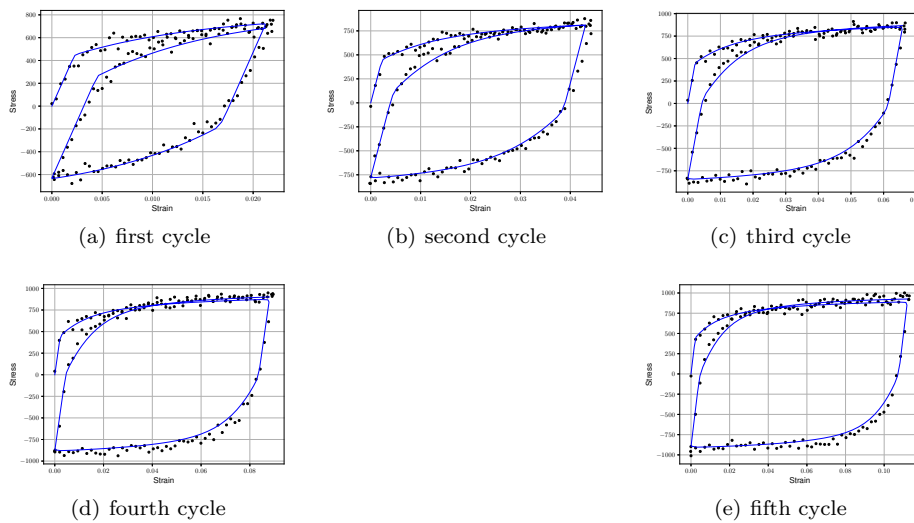
Fig. 25 Area results with noise for kinematic hardening parameter identification.

(a) first cycle

(b) second cycle

(c) third cycle

(d) fourth cycle

(e) fifth cycle
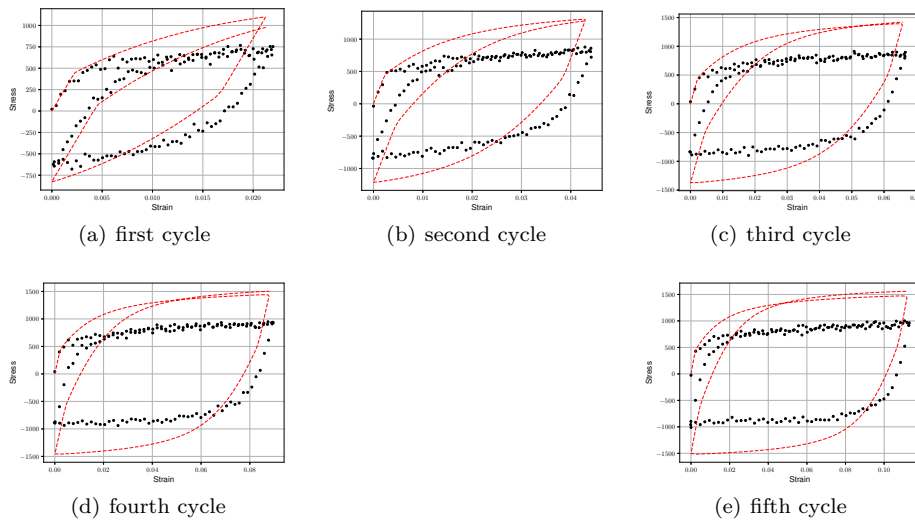
Fig. 26 PCM results with noise for kinematic hardening parameter identification.

(a) first cycle

(b) second cycle

(c) third cycle

(d) fourth cycle

(e) fifth cycle
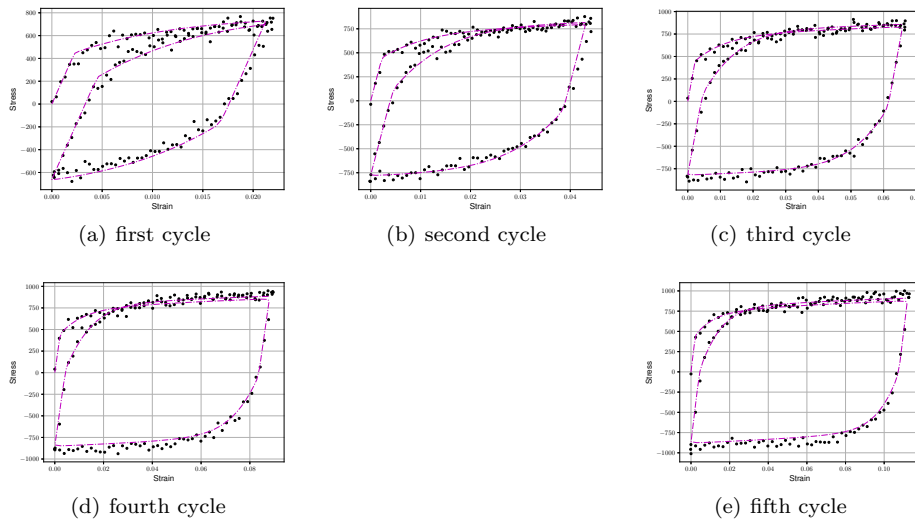
Fig. 27 Discrete Fréchet results with noise for kinematic hardening parameter identification.

(a) first cycle   (b) second cycle   (c) third cycle

(d) fourth cycle   (e) fifth cycle
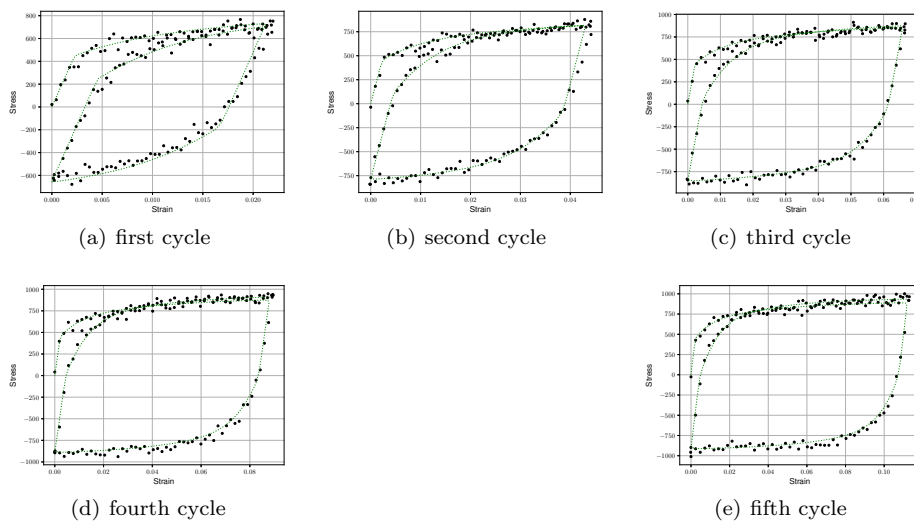
Fig. 28 DTW results with noise for kinematic hardening parameter identification.

(a) first cycle   (b) second cycle   (c) third cycle
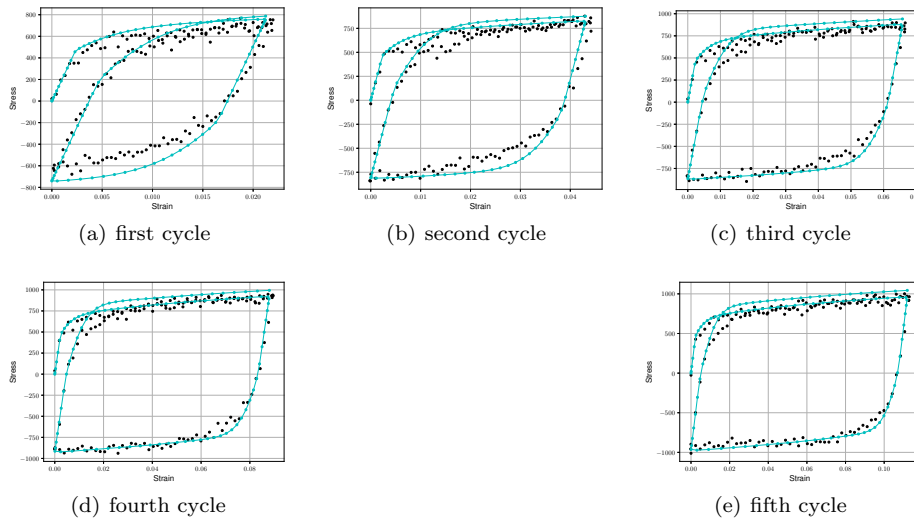
(d) fourth cycle   (e) fifth cycle

Fig. 29 Curve Length results with noise for kinematic hardening parameter identification.